JOURNAL OF MATERIALS SCIENCE: MATERIALS IN MEDICINE 3 (1992) 65–74

Phase transformation in carbon-coated nitinol, with application to the design of a prosthesis for the reconstruction of the anterior cruciate ligament

A. HEDAYAT, J. RECHTIEN*, K. MUKHERJEE‡
Department of Metallurgy, Mechanics, and Materials Science, Michigan State University, East Lansing, Michigan 48824, USA

Ultra-low temperature isotropic carbon was vapour-deposited on a near equiatomic Ti–Ni (Nitinol) alloy (49.9 at% Ti–50.1 at% Ni). The objective of the carbon coating was the induction of growth of collagenous tissue, as part of a preliminary design of a prosthesis for the reconstruction of the anterior cruciate ligament. Differential scanning calorimetry was used to study the phase transformation of carbon-coated Nitinol. X-ray diffraction and Auger electron spectroscopy were used in the study of the carbon/Nitinol interface. The results show that unannealed coatings do not inhibit the Nitinol phase transformation regardless of the thickness of the coatings. However, on heat treating the coated samples, a TiC layer forms at the carbon/Nitinol interface. The thickness of that layer increases with increasing the time of heat treatment. Surface constraint of the Nitinol by the TiC results in a marked drop in the austenitic start (A_s) and martensitic finish (M_f) temperatures of thin samples. The inhibition of both the premartensitic and martensitic transformations increases with the increase in thickness of the TiC interface.

1. Introduction

The near-equiatomic nickel–titanium alloy, Nitinol, belongs to a class of alloys that exhibits the shape-memory effect. This class includes binary alloys like Cu–Zn, Cu–Sn, Au–Cd, Ni–Al, as well as ternary systems such as Cu–Al–Ni, Cu–Zn–Si, and Ni–Ti–Cu [1]. These alloys change their shape repeatedly with heating and cooling. Consequently, they have been used in a variety of applications ranging from tubing or pipe couplings [2] to orthodontic dental arch wires [1]. Of all the shape-memory alloys, Nitinol is most commonly considered for use in biomedical applications. This is attributed to the fact that this material fulfils the two requirements of a bio-implantable material, namely biocompatibility and biofunctionability [3]. The success of Nitinol as a biomaterial has encouraged both engineers and physicians to use it in developing new prosthetic devices. For example, Nitinol is being considered for use in the treatment of scoliosis, straightening out dental malocclusions, and bone fracture fixation [1].

In this research, a new application for Nitinol in the biomedical field is proposed. The alloy will be used in the development of a prosthetic device for the reconstruction of the anterior cruciate ligament. The prosthesis is designed to eliminate the problems associated with an earlier design that used carbon fibres for the same application. Carbon fibres were utilized in this previous design because of their ability to bio-conduct collagenous tissue [4–10]. Carbon fibres are follicular, extremely brittle, and highly vulnerable to shearing forces, thus it is difficult to anchor them to tissues and bones, as they will not tolerate being knotted or stapled [11]. Fragments of the broken fibres travel to the lymph nodes [10], and excessive ligament regrowth usually occurs [12]. Further, the new tissue fibres generated tend to be straight and lack the spiral geometry that allows the natural ligament to remain taut in multiple configurations [4].

The prosthesis design suggested here for the reconstruction of the anterior crucite ligament is primarily made of Nitinol strips and filaments. A new technique for anchoring the prosthesis to the tibia and femur is proposed. This technique is based on the unique property of Nitinol to change its shape with heating and cooling. The advantages of using Nitinol in this application rather than a non-memory alloy are twofold. One advantage results from the contraction of the Nitinol wires to body temperature on warming, which causes the tibia and femur to be pulled together, and tightening of the prosthesis may be achieved. The other advantage results from the anchoring technique:

* Also affiliated with the Department of Biomechanics, College of Osteopathic Medicine, Michigan State University, East Lansing, Michigan 48824, USA.
‡ Also a member of the Composite Materials and Structures Center of Michigan State University.

0022–2461/92 $03.00 + .12

Nitinol strips to which the filaments are attached are deflected by body heat after passing through the tibia and femur. The deflection of the strips, together with the contraction of the wires, will act as a spring and is expected to counterbalance loading of the prosthesis during knee motion.

Ultra-low temperature isotropic (ULTI) carbon is also vapour deposited on the Nitinol filaments to induce the growth of collagenous tissue. ULTI carbon has the commercial name Biolite*. This class of carbon has a turbostratic structure, where the hexagonal carbon layers are arranged randomly. The material is strong and tough, and does not fail in a fatigue mode. This renders the material very useful in biomedical applications [13].

Following the implantation of the prosthesis in the knee joint, the carbon-coated filaments will be subjected to cyclic loading during physical activities. The external stresses will cause the Nitinol filaments to experience phase transformation from austenite to martensite. This phenomenon is called stress-induced martensite [14]. When the stress is removed, the body temperature will transform the martensite into austenite once again if the austenite finish temperature is less than or equal to 35 °C.

Phase transformation of Nitinol has been investigated by several researchers [14–22], and the premartensitic phase, the R-phase, has been the focus of other studies [22–38]. However, none of the studies conducted has dealt with the transformation of surface-constrained Nitinol (or other shape-memory alloys). It is the objective of this research to study the effect of surface constraint, represented by a thin (ULTI) carbon film, on the phase transformation of Nitinol.

2. Materials and methods

In this study, a near-equiatomic nickel–titanium (50.1 at % Ni–49.9 at % Ti) shape-memory alloy, Nitinol, was used. The alloy was available in the plate form, 2.5 mm thick, as well as in filament form, 0.0152 mm in diameter.

The ULTI carbon, Biolite, was vapour-deposited on the Nitinol substrates at Carbomedics Inc. (Austin, Texas) at a low pressure in a hybrid process. The process is discussed in another publication [39]. A catalyst was used to deposit the Biolite at high rates from a carbon-bearing gaseous precursor, and the temperature of the substrate was about 80 °C. Thus, the carbon was vapour deposited on austenitic Nitinol. Two thicknesses of carbon films were applied to two different batches of Nitinol samples. The film thicknesses were 0.15 and 0.3 μm.

To prepare samples for differential scanning calorimetry (DSC) measurements, the thickness of the Nitinol plates was reduced from 2.5 to 0.6 mm using a Fenn rolling machine. Due to the explosive fracturing of Nitinol on cold working, the plates were hot rolled. The samples were wet-ground through 600 grit SiC paper, and then cut with a shearing device to small pieces, each weighing 25 mg on average. The samples were placed in an alumina crucible and vacuum annealed at 550 °C for 1 h in a Centorr vacuum furnace. They were rinsed ultrasonically in acetone, and only half of the samples were coated with carbon. The film thicknesses were 0.15 and 0.3 μm. Moreover, in order to promote the interfacial bond between the ULTI carbon and the Nitinol, some of the coated samples were heat treated in vacuum at 700 °C for 3 h and others for 6 h. Uncoated samples were subjected to the same heat treatments, to establish a reference for the comparison of experimental results between coated and uncoated samples tested by DSC.

DSC measurements of the coated and uncoated samples were performed using a DuPont 910 differential scanning calorimeter that is equipped with a 9900 computer/thermal analyser. The samples were placed in DuPont 900786–901 aluminum pans and covered with 900779–901 aluminum lids. Pure cathodic nickel, which has approximately the same thermal mass as the Nitinol samples, was used as the reference material.

Coated and uncoated Nitinol samples with identical thermomechanical histories were tested using DSC. The samples were thermally cycled between − 40 and 80 °C. The temperature stability was maintained by using a liquid nitrogen cold stage. The ramp of heating and cooling for all samples was fixed at 5 °C min^{-1}. A General Electric model XRD-5 X-ray diffractometer was used to identify the phases present in the coated and the uncoated Nitinol samples. A copper target was used at 25 kV and 22 mA. The diffraction pattern was recorded for the 2Θ angle from 15 to 95° at a scanning rate of two degrees per minute.

The Nitinol samples used in X-ray analysis were prepared following the same procedure as that applied to the DSC samples. However the samples used in the X-ray study had a larger area. Coated and uncoated samples with the same thermomechanical histories were heat treated in vacuum at 700 °C for 1, 3 and 6 h before XRD analysis. The vacuum annealing ensured that all samples, coated and uncoated, were fully transformed into austenite.

Scanning electron microscopy (SEM) was utilized in the study of the topography of the vapour deposited ULTI carbon on the Nitinol substrates. Nitinol substrates were cut from a 2.5-mm-thick plate using a Buehler Isomet low-speed diamond saw. The samples were wet-ground through 600 grit SiC paper and polished through 0.3 μm alumina. The samples were then rinsed ultrasonically in acetone, dried, and ULTI carbon was vapour-deposited on them. The surfaces of coated specimens that were not heat treated, together with other coated specimens that were vacuum heat treated at 700 °C for 1, 3 and 6 h, were examined using the SEM. The microscope used was a Hitachi S-415A, and was operated at 25 kV.

The characteristics of the surfaces and interfaces of the carbon-coated Nitinol samples were studied by Auger electron spectroscopy (AES). Coated specimens, identical in their thermomechanical histories, were analysed with a Perkin–Elmer PHI 660 scanning

* Registered trademark.

Auger microprobe equipped with a PHI 04-303 sputter ion gun. The analysis was performed on coated samples that were not heat treated, as well as on coated samples heat treated in vacuum at 700 °C for 1, 3 and 6 h. Depth profiling was applied to determine the chemical profiles normal to the surface of the carbon-coated substrates. The AES was operated at a base vacuum of 2×10^{-10} mbar, an electron beam voltage of 30 kV, and an ion beam voltage of 3.5 kV. Argon was used to sputter an area of 2×2 mm at a sputter pressure of 1×10^{-8} mbar. The data were analysed using an Apollo 3500 workstation equipped with PHI AES software.

The objective of the vapour deposition of carbon was the induction of growth of collagenous tissue over carbon-coated surfaces. Thus in a preliminary biological experiment unannealed carbon-coated Nitinol filaments were implanted in a canine pelvic knee. Nitinol filaments, 0.076 mm in diameter, were annealed in vacuum at 550 °C for 1 h. The filaments were rinsed ultrasonically in acetone, and then a thin film (0.3 μm) of ULTI carbon was vapour-deposited on them. The coated filaments were sterilized by gaseous ethylene oxide before their introduction into the dog's knee joint.

The surgical technique was similar to that followed to stabilize ruptured cruciate knees with fascia lata tissue in the dog. The canine, a female large breed (52 lb) was conditioned for 1 month prior to surgery. One stifle joint was asceptically surgically approached, and tunnels were drilled in the condyles of the tibia and femur. A long band of fascia lata tissue was cut from the lateral side of the thigh and pulled through the tunnels in the femur and tibia. Prior to the placement of the tissue through the bone, carbon-coated filaments were incorporated with it in such a manner that the filaments would be located in the stifle joint. After the tissue was removed from the anterior of the tibia, it was anchored to the patellar ligament. The wound was closed and the operated knee joint was then wrapped in soft padded bandage. After surgery, the dog was housed in a ward with no restriction to its motion. It was then euthanized 30 days post-operatively with a T-61 intravenous injection, and the knee joint was harvested.

The growth of collagenous tissue on the carbon-coated Nitinol filaments were studied by SEM after removal from the dog's knee. To stop any degeneration of the harvested knee joint, it was immersed in 10% formalin for 3 days. Cross-section and longitudinal cuts of the coated filaments adjacent to the patellar tendon and the surrounding tissue were made. The sections were dehydrated at room temperature in a series of ethyl alcohol/water mixtures with increasing concentrations of alcohol. The starting concentration was 70 vol % alcohol and the final was 100 vol %, with 10% increments. The specimens were immersed in each concentration for 1 h. Treatment of the tissue with the 100% alcohol concentration was repeated three times to make sure that dehydration was complete. At this stage, the tissue with the embedded filaments had to be critically dried to remove any water present. Thus a critical point dryer using CO_2 gas was employed. The filaments and annexed tissue were then cut to smaller pieces and glued to aluminum SEM stubs using super glue. Since the tissue is non-conductive, it had to be sputter coated with gold before examination. The microscope used was a Hitachi S-415A scanning electron microscope, operated at 25 kV.

3. Results

3.1. Differential scanning calorimetry

A typical DSC curve of a TiNi shape-memory alloy annealed for 1 h at 550 °C and thermally cycled for the first time is characterized with a single peak in each of the cooling and heating cycles. The peak associated with the cooling cycle is exothermic and is characterized by martensitic start and finish temperatures, M_s and M_f, respectively. The peak associated with the heating cycle, on the other hand is endothermic, and is characterized by an austenitic start and finish temperatures, A_s and A_f, respectively. In both cases, the area under the curve is the enthalpy of the transformation, and is denoted by ΔH. Table I summarizes the data for the NiTi alloy under study, which has a composition of 50.1 at % Ni–49.9 at % Ti. It is noted that the enthalpy of transformation of the cooling cycle is almost equal to the enthalpy of transformation of the heating cycle.

Thermal cycling of Nitinol caused two exothermic peaks to form in the cooling cycle. The first peak to appear is associated with the premartensitic reaction and the formation of the R-phase, while the second is associated with the martensitic phase. Experimental results showed that the more times the Nitinol was thermally cycled, the lower were the martensitic start and finish temperatures.

Carbon-coated Nitinol samples which were not subjected to heat treatment following the coating process did not undergo any changes of the alloy's transformation temperatures or of the heats of transformation in either the heating or the cooling cycle. Variation of the thicknesses of the coatings did not affect the transformation temperatures of Nitinol. The heats of transformation (ΔH) of uncoated and coated Nitinol are given in Table II. The data are given for two different thicknesses of Biolite, 0.15 and 0.3 μm. For the coated samples that were not heat treated following the coating process, two distinct characteristics are associated with the phase transformation. The first is that the carbon coating does not inhibit the formation of the R-phase; the second is that thermal cycling of the coated Nitinol caused parts of the coating to flake out. This meant that the carbon coating

TABLE I Thermodynamic data for a near-equiatomic NiTi alloy (50.1 at % Ni–49.9 at % Ti)

M_s	300 K
M_f	271 K
A_s	296 K
A_f	327 K
$\Delta H_{cooling}$	23.74 J g^{-1}
$\Delta H_{heating}$	24.17 J g^{-1}

TABLE II Heats of transformation (ΔH) of coated and uncoated Nitinol in the unannealed state ($J\,g^{-1}$). Substrate thickness = 600 μm.

Cycle	Uncoated		Coated			
			0.15 μm		0.3 μm	
	Cooling	Heating	Cooling	Heating	Cooling	Heating
1	20.09	19.53	23.54	23.32	24.12	24.32
10	20.00	22.16	23.30	23.30	23.61	22.49
20	19.81	22.76	22.70	22.70	23.0	21.76
30	19.14	22.65	22.80	22.80	23.03	20.96
40	18.82	22.77	22.59	22.59	23.01	20.90

vapour-deposited without subsequent annealing was poorly bonded to the Nitinol substrates.

The coated samples were annealed to promote the interfacial bond between the TiNi and the ULTI carbon coating. To establish a reference for the comparison of the DSC measurements of the coated samples, uncoated Nitinol samples were subjected to the same heat treatment and tested using DSC. Fig. 1a and b shows the DSC curve in the first cooling cycle for an uncoated, and 0.3 μm carbon-coated samples, respectively, heat treated for 3 h at 700 °C. It is shown that although the M_s temperature remains the same for both the coated and uncoated samples, the M_f temperature for the coated and annealed sample dropped by about 20 °C in comparison to the uncoated sample. Fig. 2 shows the DSC curve of the first heating cycle of an uncoated Nitinol sample (a), and a 0.3-μm carbon-coated sample (b), each heat treated for 3 h at 700 °C. It is shown that the A_f temperature for the coated and uncoated samples remains unchanged. However, in case of the coated sample, the A_s temperature dropped by about 20 °C in comparison to the uncoated one.

When DSC measurements were made for uncoated and 0.3-μm carbon-coated samples annealed at 700 °C for 6 h, similar results were obtained. Fig. 3a and b shows the DSC cooling curve of the first cycle for uncoated and coated Nitinol samples, respectively. Fig. 4 shows the DSC curves for the heating cycle. From both figures it can be seen that for the constrained samples, the M_f and A_s temperatures dropped markedly, while the M_s and A_f temperatures were unchanged. The uncoated and coated samples that were heat treated at 700 °C for 3 and 6 h were cycled to study the effect of surface constraint on the R-phase. It was found that the heat treatment promoted the surface constraint and inhibited the formation of the R-phase. This effect is illustrated in Fig. 5a and b which shows DSC curves of the fortieth cooling cycle

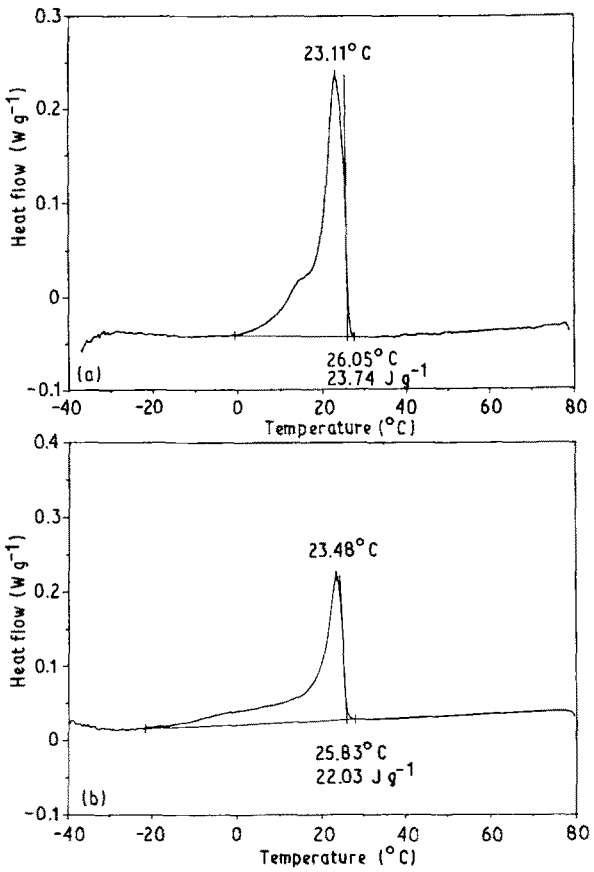

Figure 1 DSC curves of the first cooling cycle of Nitinol samples. (a) Uncoated and annealed at 700 °C for 3 h; (b) coated with a 0.3-μm carbon film and annealed at 700 °C for 3 h.

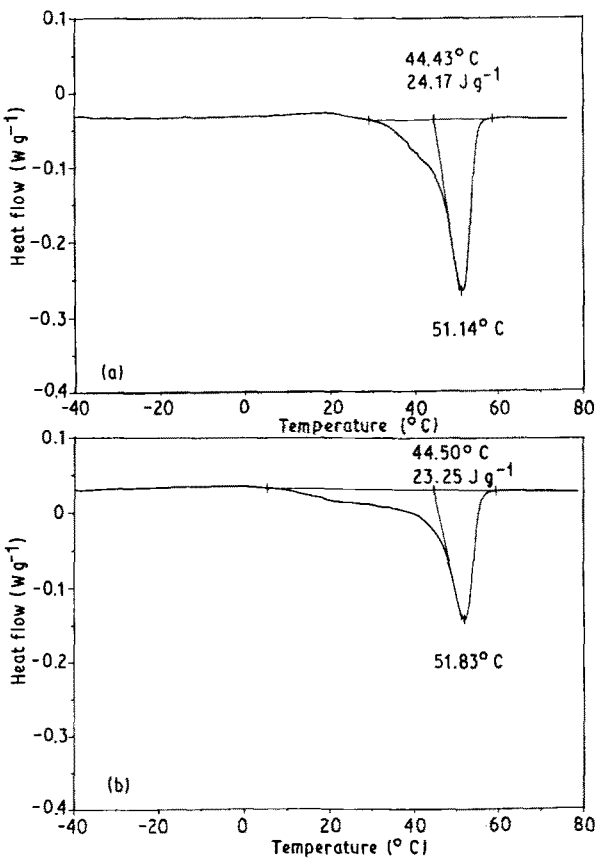

Figure 2 DSC curves of the first heating cycle of Nitinol samples. (a) Uncoated and annealed at 700 °C for 3 h; (b) coated with a 0.3-μm carbon film and annealed at 700 °C for 3 h.

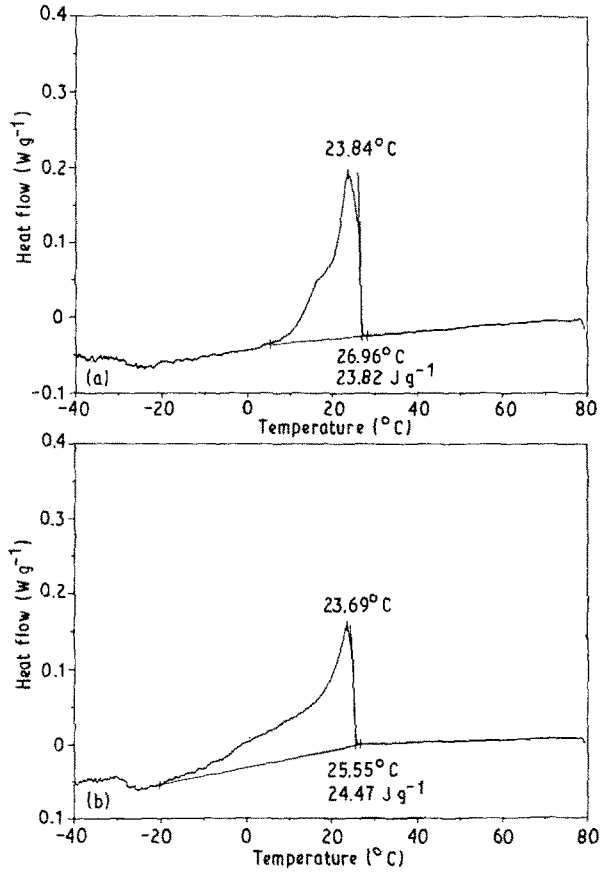

Figure 3 DSC curves of the first cooling cycle of Nitinol samples. (a) Uncoated and annealed at 700 °C for 6 h; (b) coated with a 0.3-μm carbon film and annealed at 700 °C for 6 h.

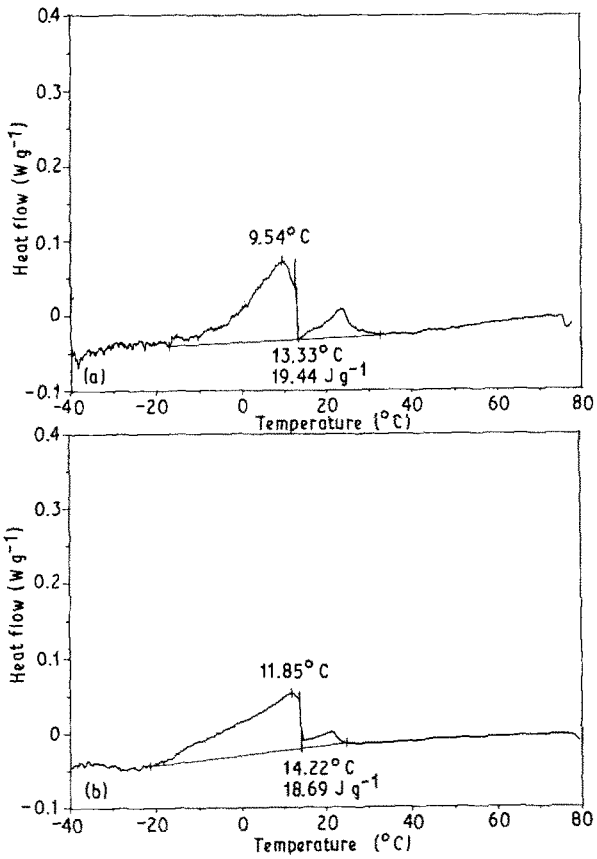

Figure 5 DSC curves of the 40th cooling cycle of Nitinol samples. (a) Uncoated and annealed at 700 °C for 6 h; (b) coated with a 0.3-μm carbon film and annealed at 700 °C for 6 h.

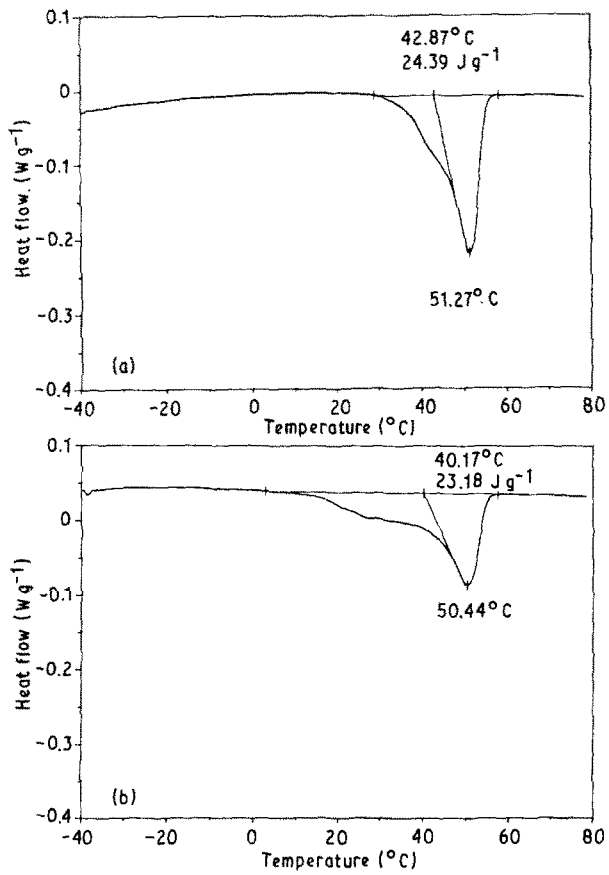

Figure 4 DSC curves of the first heating cycle of Nitinol samples. (a) Uncoated and annealed at 700 °C for 6 h; (b) coated with a 0.3-μm carbon film and annealed at 700 °C for 6 h.

of an uncoated and a 0.3-μm carbon-coated Nitinol sample, respectively. Both samples were heat treated at 700 °C for 6 h.

3.2. X-ray analysis

X-ray analysis was carried out for the uncoated and 0.3-μm carbon-coated Nitinol. The carbon coating has a turbostratic, semi-crystalline structure. Thus no peaks were recorded from the carbon film. When the carbon-coated Nitinol is annealed, the thickness of TiC formed at the carbon/Nitinol interface increases and consequently peaks of TiC appear in the X-ray diffraction pattern of annealed carbon-coated Nitinol. Fig. 6 shows the diffraction pattern of a 0.3-μm carbon-coated sample annealed for 3 h at 700 °C. The intensities of the TiC peaks are small in comparison with the TiNi peaks. Annealing of the carbon-coated samples at the same temperature (700 °C) for a longer period of time (6 h) caused the TiC peaks to intensify, as illustrated in Fig. 7.

3.3. Scanning electron microscopy of the carbon-coated TiNi alloy

The electron microscope was used in the scanning mode to evaluate both the microstructure and topography of the uncoated and carbon-coated Nitinol samples. The vapour-deposited ULTI carbon film was found to form a continuous film on the Nitinol surface. Thicknesses of the carbon film up to 0.3 μm did

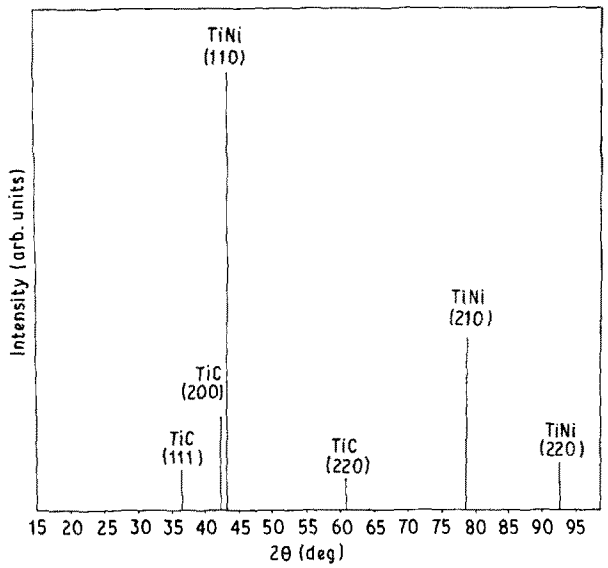

Figure 6 X-ray diffraction pattern of a 0.3-μm carbon-coated Nitinol sample heat treated at 700 °C for 3 h after coating.

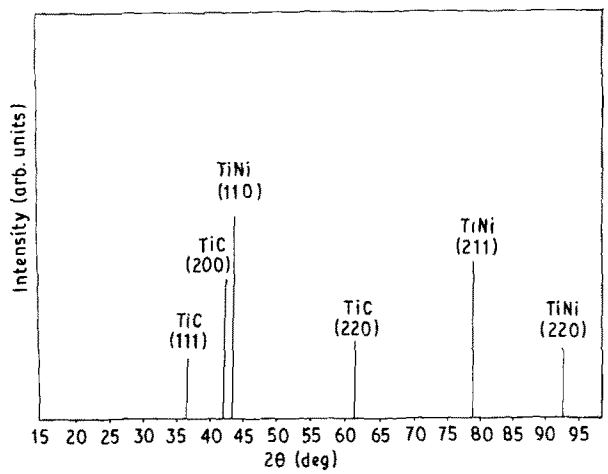

Figure 7 X-ray diffraction pattern of a 0.3-μm carbon-coated Nitinol sample heat treated at 700 °C for 6 h after coating.

not change the topography of Nitinol, and had no microstructural features. SEM photomicrographs of unannealed Nitinol are shown in Fig. 8a and b for uncoated and coated samples, respectively. Comparison of the microstructure of both micrographs proves that the coating is continuous and does not change the topography of the Nitinol samples. When uncoated and coated Nitinol samples were annealed, the carbon film remained continuous and did not change the topography of the Nitinol surface.

3.4. Auger electron spectroscopy

Elemental analysis of the carbon-coated Nitinol was carried out using Auger electron spectroscopy. The analysis was done for 0.3-μm carbon-coated Nitinol samples that were unannealed, as well as for coated samples that were annealed for 1, 3 and 6 h. Concentration profiles measured with the depth profiling technique were also obtained for these samples.

Fig. 9 shows a depth profile of an annealed, 0.3-μm carbon-coated sample, illustrating how carbon is concentrated at the surface, its concentration dropping distal to the carbon/Nitinol interface. On the other hand, both nickel and titanium are concentrated in the bulk of the material, and are depleted at the surface of the sample. Considering the carbon film thickness, it is estimated that the sputtering rate of the carbon film was about 0.025 μm min^{-1}. Fig. 10 shows the Auger spectrum of the sample after 1 min argon sputtering. The spectrum shows that only carbon is present at the surface. Analysis of the carbon signal shows that it is present in the elemental form.

Auger analysis was also carried out on 0.3-μm carbon-coated samples annealed at 700 °C for 1, 3 and 6 h. Experimental results show that the annealing for 1 h at 700 °C broadened the TiC region at the carbon/

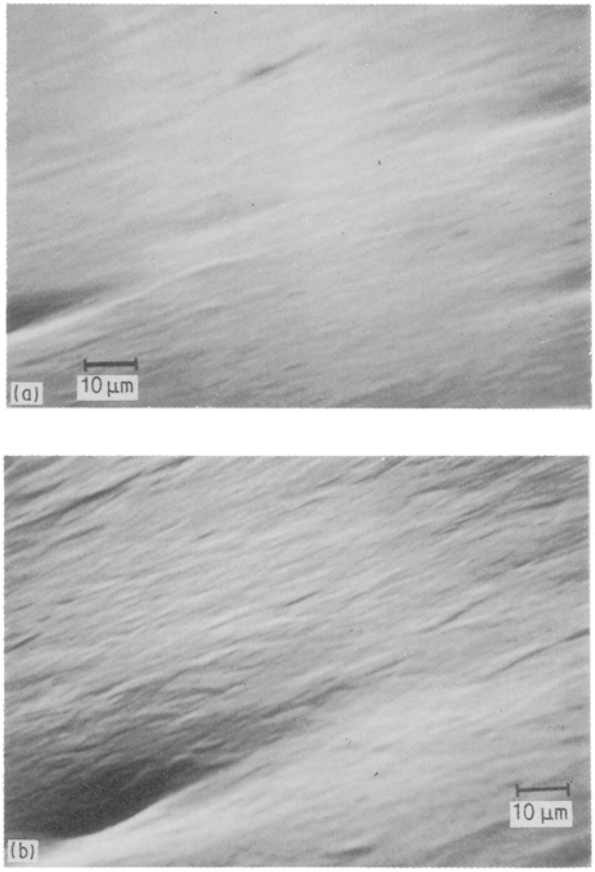

Figure 8 SEM photomicrograph of (a) an uncoated, unannealed Nitinol sample; (b) unannealed 0.3-μm carbon-coated Nitinol sample.

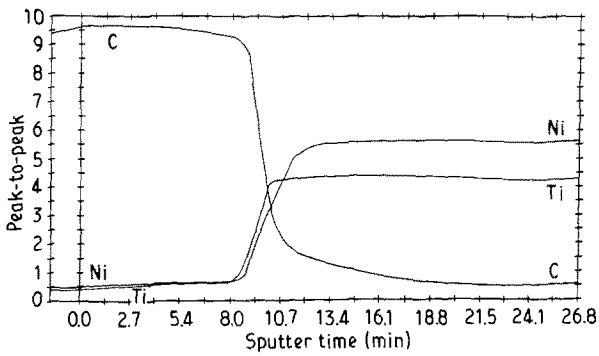

Figure 9 Depth profile of an unannealed 0.3-μm carbon coated Nitinol sample.

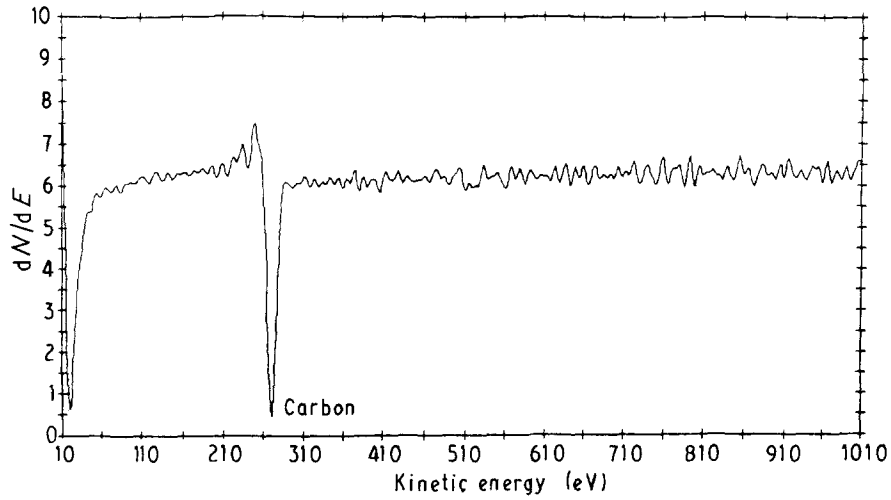

Figure 10 Auger signal of an unannealed 0.3-μm carbon coated Nitinol sample after 1 min argon sputtering.

Nitinol interface. The Auger spectrum for the sample annealed for 3 h showed that the carbon in the elemental form still existed at the surface. It was deduced that the longer heat treatment broadened the TiC region at the carbon/Nitinol interface, as compared to 1 h annealing.Fig. 11a is an SEM photomicrograph of the argon-sputtered surface of an unannealed carbon-coated Nitinol sample. The contrast between the carbon coating and the TiNi phase shows a sharp interface area between the carbon film and the substrate. Fig. 11b, on the other hand, is an SEM micrograph showing a broad TiC interface region in a carbon-coated sample that was annealed for 3 h at 700 °C.

A 6-h anneal was sufficient to make the 0.3-μm carbon film react with the substrate to form TiC at the surface of the Nitinol substrate. This is illustrated in Fig. 12 which shows the Auger spectrum after 1 min argon sputtering. Analysis of the carbon signal in Fig. 12 shows that it exists in the compound form,

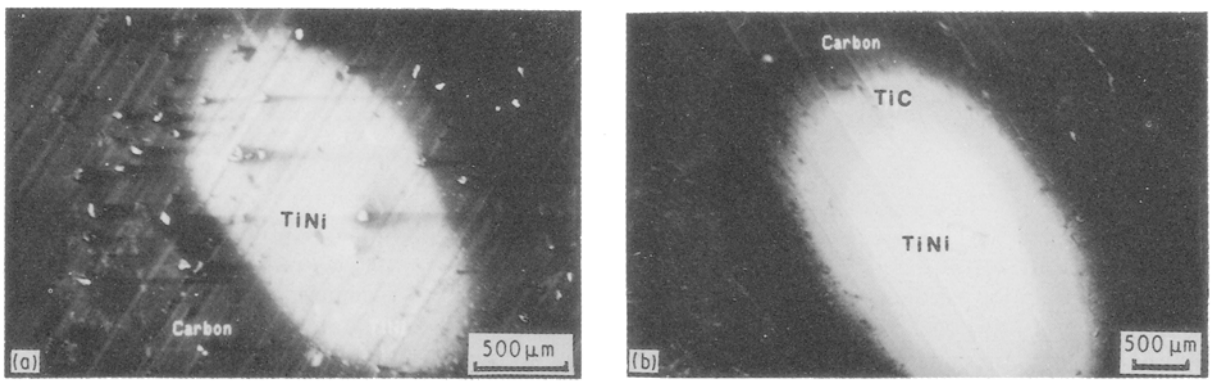

Figure 11 SEM photomicrograph of (a) unannealed 0.3-μm carbon-coated Nitinol after 26 min argon sputtering; (b) 0.3-μm carbon-coated Nitinol annealed at 700 °C for 3 h after 40 min argon sputtering.

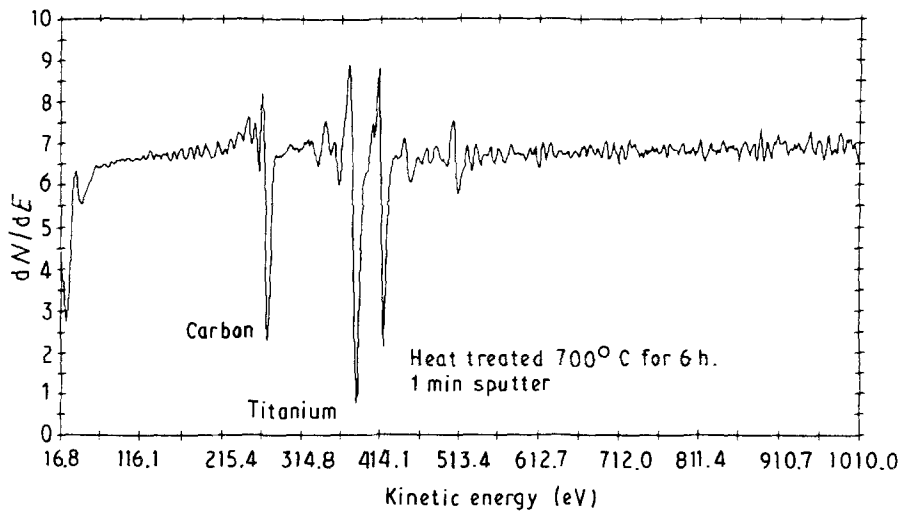

Figure 12 Auger signal after 1 min argon sputtering of a 0.3-μm carbon-coated Nitinol sample annealed at 700 °C for 6 h after coating.

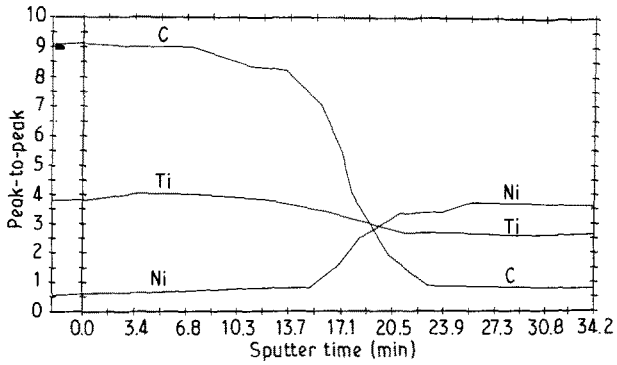

Figure 13 Depth profile of a 0.3-μm carbon-coated Nitinol sample annealed at 700 °C for 6 h.

TiC. Fig. 13, which is a depth profile of the sample, also shows that titanium is present at the surface with carbon.

3.5. Biological evaluation of the carbon-coated Nitinol

SEM examination of a wire section taken from an area adjacent to the patellar tendon during surgery showed the presence of islands of reticular collagen on the surface of the carbon-coated filaments (Fig. 14). SEM examination of the carbon-coated Nitinol filaments also showed cracks in the carbon coating, probably originating with successive loading of the filament in the dog's knee (Fig. 15). The presence of these cracks indicates poor bonding between the Biolite and the Nitinol when unannealed, suggesting that annealing is essential for keeping the coating and the Nitinol substrate intact.

4. Discussion

4.1. Phase transformation of Nitinol

Phase transformation studies showed that the constraint in the 0.3-μm carbon-coated and annealed Nitinol samples, represented by TiC, caused both the M_f and the A_s temperatures to drop markedly. The constraint also suppressed the formation of the R-phase. It is significant that the phase transformation of Nitinol is affected by the ratio of constraint thickness to sample thickness. This can be illustrated by comparing the DSC results for unannealed and annealed carbon-coated Nitinol samples. With annealing, a TiC layer was formed at the carbon/Nitinol interface. The thickness of this layer increased with the time of annealing until it was capable of constraining the surface of Nitinol and suppressing its phase transformation.

The surface constraint was found to affect the driving force of the phase transformation of Nitinol. For the martensitic transformation, M_s is the same for both the constrained and unconstrained sample. However, as the transformation proceeds, the constraint opposes the driving force in the surface-constrained sample, causing it to be lower than that for the unconstrained sample. In order to overcome the constraint and the strain energy associated with it, the constrained sample has to be supercooled to achieve the same driving force required to complete

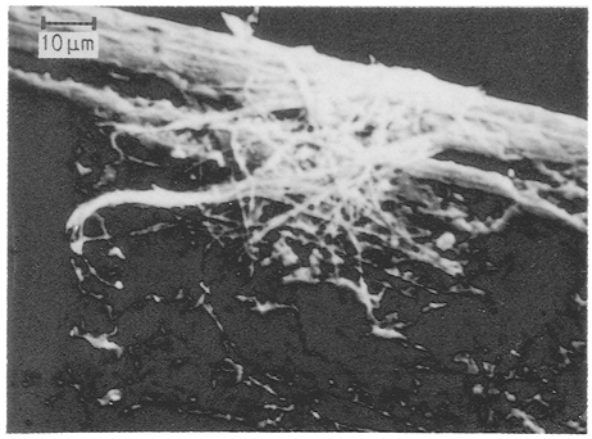

Figure 14 SEM photomicrograph of collagen islands on the surface of carbon-coated Nitinol filaments (× 1000).

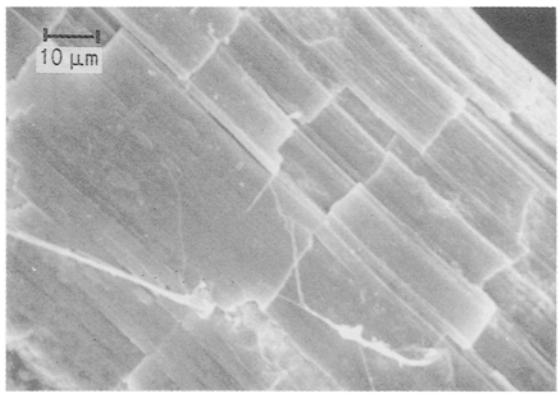

Figure 15 SEM photomicrograph of cracks in the carbon-coated Nitinol filaments (× 1000).

the transformation as in the unconstrained sample. Thus, at any temperature during the martensitic transformation other than M_s, the net driving force for the constrained sample is lower than that for the unconstrained one. It is deduced that for surface-constrained samples, martensitic transformation starts in the bulk and proceeds to the surface with the decrease in temperature.

In the martensite-to-parent phase transformation, the A_s temperature for the surface-constrained sample is lower than that of the unconstrained one. This is attributed to the fact that there is an increased amount of strain energy associated with the surface-constrained sample during the martensitic transformation. The release of this stored energy assists in the reverse transformation, causing it to start earlier, at a lower temperature. Thus the driving force is greater in the constrained sample in the reverse transformation than in the unconstrained one, at any temperature during the reverse transformation. Since the accommodation strain is largest for the martensite plates formed near the constrained surface, the reverse transformation of the surface-constrained sample starts at or near the surface and proceeds to the bulk with the increase in temperature.

4.2. Design of a prosthesis for the reconstruction of the anterior cruciate ligament

SEM figures of the harvested carbon-coated filaments

showed that islands of reticular collagen formed on the carbon surface within 30 days. This finding, combined with the fact that Nitinol is a biofunctional material exhibiting the shape-memory effect, led to the design of a prosthetic device to be used in the reconstruction of the anterior cruciate ligament. The design envisioned uses the unique ability of Nitinol to change its shape with temperature. The Nitinol alloy chosen should have an austenitic finish temperature of about 35 °C, below body temperature. Fig. 16 shows the proposed design of the prosthesis. One prosthesis has the ends deflected to illustrate the anchoring position with the tibia and femur when the Nitinol transforms with body temperature.

The components of the prosthesis are illustrated in Fig. 17. It consists of two hollow cylindrical ends connected with the carbon-coated filaments. There are two upset horizontal pins in each hollow end: the lower is for filament attachment, and the upper is for surgical handling while pulling the ends of the prosthesis through the bones. The filaments will be twisted in a spiral configuration similar to that of the anterior cruciate ligament.

Before their attachment to the hollow cylindrical ends of the prosthesis, and prior to their being coated with Biolite, the filaments will be subjected to thermomechanical training. They will be strained below M_f by 6–8%, and with the release of loading they will be heated above A_f. This process will be repeated several times, so that once introduced into the knee and warmed to body temperature, the filaments will contract.

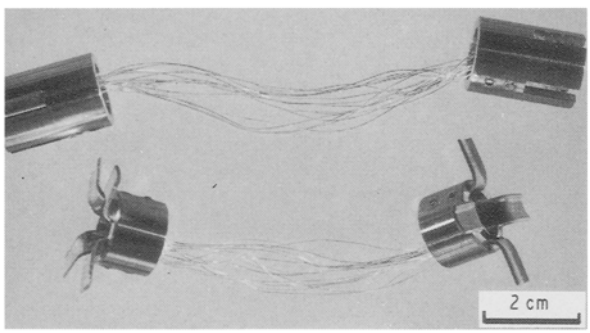

Figure 16 Proposed design of a carbon-coated Nitinol prosthesis for the reconstruction of the anterior cruciate ligament.

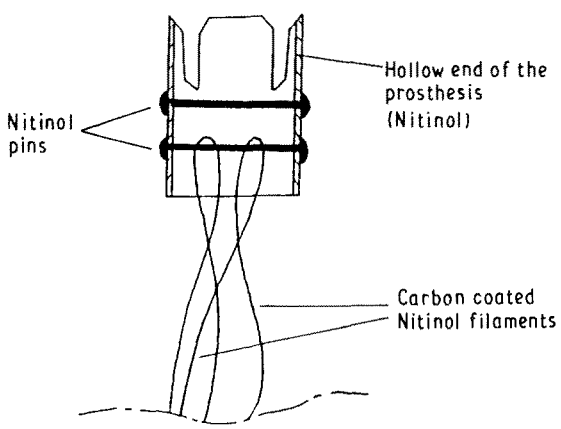

Figure 17 Design details of the prosthesis devised for the reconstruction of the anterior cruciate ligament.

Fig. 18 illustrates the method by which the prosthesis will be presented into the knee joint. After the tunnels in the condyles of the tibia and femur are drilled, a flexible scale will be introduced to measure the distance between the surfaces of the tibia and the femur at the tunnel outlets. The prosthesis of the desired length, which will be kept at low temperature before use, will then be introduced into the knee joint. To avoid transformation of the Nitinol prosthesis, the

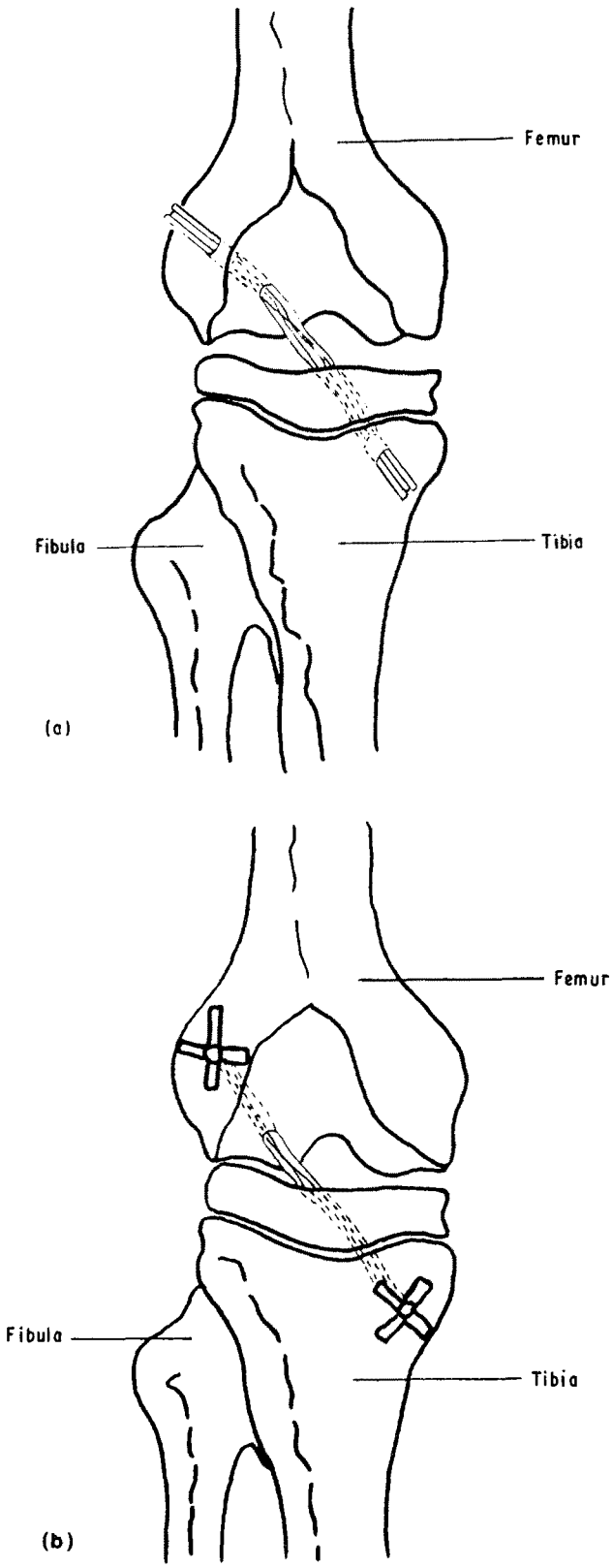

Figure 18 Prosthesis in the knee joint (a) before transformation; (b) after transformation.

knee will be cooled well below body temperature by ice packs. Fig. 18a shows the prosthesis in the untransformed configuration. The ice packs will be removed from around the knee allowing it to warm to body temperature, which will in turn heat the Nitinol prosthesis. Both ends of the prosthesis will deflect, and the anchoring of it to the tibia and femur is complete (Fig. 18b). Also, the filaments will shrink by 6–8%, thus exerting a traction force which pulls the tibia and femur together. This anchoring technique has the advantage of a spring effect that counterbalances loading of the prosthesis during knee motion, and contrasts with the other techniques where the ends of the prosthesis are fixed rigidly to the tibia and femur.

5. Acknowledgements

The authors would like to thank Dr Terrance Braden of Michigan State University for performing the surgery in this research work. Sincere gratitude is also expressed to Mr Charles Hovey of US Nitinol for supplying the Nitinol filaments used in this study, and to Dr Axel Haubold and Mr Al Beavan of Carbomedics, Inc. for coating the Nitinol substrates with Biolite. Thanks are also extended to Ms Jane Walsh for preparing the samples used in the biological evaluation of the carbon-coated samples. The authors respectfully acknowledge funding of this work through Michigan State Research Excellence Fund (REF) administered through the Composite Materials and Structures Center of Michigan State University.

References

1. K. MUKHERJEE, in "Encyclopedia of Materials Science and Engineering", edited by M. Bever (Pergamon, New York, 1986) p. 4368.
2. C. WAYMAN, in *ibid.* p. 4371.
3. L. S. CASTLEMAN and S. M. MOTZKIN, in "Biocompatibility of Clinical Impant Materials", edited by D. Williams (CRC Press, Florida, 1981) p. 129.
4. D. H. R. JENKINS, *J. Bone J. Surg.* **60B** (1978) 520.
5. D. H. R. JENKINS, I. W. FORESTER, B. McKIBBINS and Z. A. RALIS, *ibid.* **59B** (1977) 53.
6. D. WALKER, E. FITZER, G. HELBING and J. GOLDAWAY, *Trans. 3rd Ann. Mtg. (Society for Biomaterials,* 1977) 126.
7. R. NEUGEBAUER, C. BURRI, L. CLAES, G. HELBING and D. WOLTER, *Trans. 2nd Mtg. European Soc. Biomat.* (1979).
8. J. C. KENNEDY, *Clin. Orthop. Rel. Res.* **175** (1983) 125.
9. D. H. R. JENKINS, *J. Bone J. Surg.* **58B** (1976) 253.
10. N. RUSHTON, D. DANDY and C. NAYLOR, *ibid.* **65B** (1983) 308.
11. G. H. JENKINS and C. J. GRIGSON, *J. Biomed. Mater. Res.* **13** (1979) 371.
12. I. FORSTER, in "Natural and Living Biomaterials" edited by G. Hastings and P. Ducheyne (CRC Press, Florida, 1984) p. 119.
13. A. HAUBOLD *et al.*, "Biocompatibility of Clinical Implant Materials", edited by D. Williams (CRC Press, Florida, 1981).
14. K. MUKHERJEE, S. SIRCAR and N. DAHOTRE, *Mater. Sci. Engng* **74** (1985). 75.
15. H. TONG and C. WAYMAN, *Acta Met.* **22** (1974) 887.
16. *Idem, ibid.* **23** (1975) 209.
17. W. JOHNSON, J. DOMINGUE and S. REICHMAN, *J. de Phys.* **43** (1982) 285.
18. J. KWARCIAK, Z. LEKSTON and H. MORAWIEC, *J. Mater. Sci.* **22** (1987) 2341.
19. R. WASILEWSKI, S. BUTLER and J. HANLON, *Met. Sci. J.* **1** (1967) 104.
20. G. AIROLDI, B. RIVOLTA and C. TURCO, in Proceedings of the International Conference on Martensitic Transformations (ICOMAT-86), Nara, Japan, August 1986.
21. J. KWARCIAK and H. MORAWIEC, *J. Mater. Sci.* **23** (1988) 551.
22. T. TADAKI, Y. NAKATA and K. SHIMIZU, *Trans. Jpn. Inst. Met.* **28** (1987) 883.
23. X. WU and T. KO, Proceedings of the International Conference on Martensitic Transformations (ICOMAT-86) Nara, Japan, August, 1986.
24. G. SANDROCK, *Metall. Trans.* **5** (1974) 299.
25. G. SANDROCK, A. PERKINS and R. HEHEMANN, *ibid.* **2** (1971) 2769.
26. K. CHANDRA and G. PURDY, *J. Appl. Phys.* **39** (1986) 2176.
27. K. OTSUKA, T. SAWAMURA and K. SHIMIZU, *Phys. Status Solidi* **5** (1971) 457.
28. R. WASILEWSKI, *Trans. AIME* **233** (1965) 1691.
29. R. HASIGUTI and K. IWASAKI, *J. Appl. Phys.* **39** (1968) 2182.
30. J. HANLON, S. BUTLER and R. WASILEWSKI, *Trans. AIME* **239** (1967) 1323.
31. H. BERMAN, E. WEST and A. ROZNER, *J. Appl. Phys.* **38** (1967) 4473.
32. D. DAUTOVICH, Z. MELKVI, G. PURDY and C. STAGER, *ibid.* **37** (1966) 2512.
33. C. HWANG, M. MEICHLE, M. SALAMON and C. WAYMAN, *Phil. Mag. A.* **47** (1983) 9.
34. *Idem, Phil. Mag. A.* **47** (1983) 31.
35. E. GOO and R. SINCLAIR, *Acta. Met.* **33** (1985) 1717.
36. C. WAYMAN, in Proceedings of the International Conference on Martensitic Transformations (ICOMAT-86), Nara, Japan, August 1986.
37. S. MIYAZAKI and C. WAYMAN, *ibid.*
38. S. MIYAZAKI and C. WAYMAN, *Acta. Met.* **36** (1988) 181.
39. A. HAUBOLD, in "Encyclopedia of Materials Science and Engineering", edited by Michael Beuer (Pergamon, New York, 1986) p. 514.

Received 15 October
and accepted 31 October 1990